

Measure transport with kernel mean embeddings

L. Wang* and N. Nüsken†

Department of Mathematics
King's College London

January 24, 2024

Abstract

Kalman filters constitute a scalable and robust methodology for approximate Bayesian inference, matching first and second order moments of the target posterior. To improve the accuracy in nonlinear and non-Gaussian settings, we extend this principle to include more or different characteristics, based on kernel mean embeddings (KMEs) of probability measures into their corresponding Hilbert spaces. Focusing on the continuous-time setting, we develop a family of interacting particle systems (termed *KME-dynamics*) that bridge between the prior and the posterior, and that include the Kalman-Bucy filter as a special case. A variant of KME-dynamics has recently been derived from an optimal transport perspective by Maurais and Marzouk [29], and we expose further connections to (kernelised) diffusion maps, leading to a variational formulation of regression type. Finally, we conduct numerical experiments on toy examples and the Lorenz-63 model, the latter of which show particular promise for a hybrid modification (called Kalman-adjusted KME-dynamics).

1 Introduction

The task of replicating a time-discrete transition or a time-continuous flow of probability measures by a system of interacting particles is a ubiquitous challenge in computational statistics and machine learning. In a Bayesian context, we might be presented with samples $(X_0^i)_{i=1}^N$ from the prior π_0 , challenged to transform those into samples $(X_1^i)_{i=1}^N$ from the posterior π_1 . In this paper, we will focus on a variant of this problem in (artificial) continuous time, and consider the curve $(\pi_t)_{t \in [0,1]}$ of distributions

$$\pi_t = \frac{e^{-th}\pi_0}{Z_t}, \quad t \in [0, 1], \quad (1)$$

see, for example, [20, 39]. In (1), the function $h : \mathbb{R}^d \rightarrow \mathbb{R}$ stands for the negative log-likelihood (we suppress the dependence on observed data in the notation), and the normalising constants are given by $Z_t = \int_{\mathbb{R}^d} e^{-th} d\pi_0$. For $t = 1$, we thus recover Bayes' formula, and (1) provides an interpolation between the prior and the posterior, where the likelihood is introduced in an incremental fashion.

The central problem of Bayesian posterior approximation may be approached by constructing a dynamical evolution governed by

$$dX_t = a_t(X_t, \rho_t) dt + \sigma_t(X_t, \rho_t) dW_t, \quad X_0 \sim \rho_0 = \pi_0, \quad (2)$$

choosing the coefficients a_t and σ_t in such a way that the corresponding distributions $\rho_t = \text{Law } X_t$ match π_t as closely as possible, for all $t \in [0, 1]$. We stress the fact that a_t and σ_t are allowed to depend on the law ρ_t , lending additional flexibility to the framework. Given appropriate coefficients, an interacting-particle and discrete-time approximation of (2) yields an implementable algorithm that

*linfeng.2.wang@kcl.ac.uk

†nikolas.nusken@kcl.ac.uk

produces approximate samples from π_1 .

The Kalman paradigm. Enforcing strict equality in $\rho_t = \pi_t$, $t \in [0, 1]$ is ambitious, as a_t and σ_t typically depend on ρ_t and h through high-dimensional PDEs, see, e.g. eq. (11) in [39] or eq. (9) in [20]. To increase scalability and reduce computational burden, it is thus reasonable to require equivalence between (1) and (2) only according to certain characteristics. The prototypical example is to match first and second moments between ρ_t and π_t (see [5, Chapter 3]), leading to closed-form expressions for a_t and σ_t , and to the celebrated family of Kalman filters [10, 40, 25, 40]. Empirically, Kalman-type methodologies perform robustly and with a moderate computational budget in high-dimensional settings, but the restriction to first and second moments renders them approximate when nonlinearity and/or non-Gaussianity is present, and they are thus unreliable in highly complex data assimilation scenarios.

Embedding probability distributions. In this work, we follow an abstract version of the Kalman principle and consider mappings of the form

$$\Phi : \mathcal{P}(\mathbb{R}^d) \rightarrow \mathcal{H}, \quad (3)$$

from the set of probability measures $\mathcal{P}(\mathbb{R}^d)$ to an appropriate Hilbert space \mathcal{H} . The space \mathcal{H} should be thought of as containing the information $\Phi(\rho)$ that we would like to retain from a probability measure $\rho \in \mathcal{P}(\mathbb{R}^d)$. Accordingly, we then impose $\Phi(\rho_t) = \Phi(\pi_t)$, a requirement often considerably weaker than $\rho_t = \pi_t$.

Kernel mean embeddings. Throughout this work, we focus on the case when \mathcal{H} is the reproducing kernel Hilbert space (RKHS) \mathcal{H}_k associated to a positive definite kernel $k : \mathbb{R}^d \times \mathbb{R}^d \rightarrow \mathbb{R}$, and Φ is the corresponding kernel mean embedding (KME) Φ_k , see [31] for an overview (we summarise relevant background in Section 2). For the specific choice $k_2(x, y) = (x^\top y + 1)^2$, the corresponding RKHS \mathcal{H}_{k_2} is finite-dimensional, containing information precisely about first and second order moments encoded in the KME Φ_{k_2} . Unsurprisingly, therefore, our approach based on (3) recovers specific forms of Kalman filters for the choice $\mathcal{H} = \mathcal{H}_{k_2}$, as we demonstrate below in Section 3.2.

Leveraging the generality of (3), it is plausible to remedy the downsides of standard Kalman filters by considering larger target spaces than \mathcal{H}_{k_2} , enhancing the expressiveness of the map Φ . Indeed, *characteristic* kernels (see Definition 2.1 below) allow full recovery of $\rho \in \mathcal{P}(\mathbb{R}^d)$ from $\Phi_k(\rho) \in \mathcal{H}_k$, the RKHS in this case necessarily being infinite-dimensional. Those kernels represent a full nonparametric description of probability measures through their KMEs, and therefore in principle lead to exact Bayesian inference schemes. A judicious kernel choice (possibly ‘in between’ k_2 and a characteristic kernel) therefore holds the promise of striking a balance between accuracy and computational tractability.

1.1 Structure and background

Outline and contributions. To develop our framework around (3), we proceed as follows. In Section 2 we survey relevant background on positive definite kernels, reproducing kernel Hilbert spaces, and kernel mean embeddings. In Section 3.1, we detail the construction of our proposed KME-dynamics, culminating in Algorithm 1. In Section 3.2, we establish the connection between KME-dynamics and the continuous-time Kalman-Bucy filter through the quadratic kernel k_2 . Section 4 exposes connections to related work, in particular to diffusion maps, the Poisson equation, and Tikhonov regularised regression functionals. We test various aspects of KME-dynamics in numerical experiments in Section 5, including one-dimensional toy examples, a high-dimensional skew normal target, and a data assimilation task for the Lorenz-63 model system.

Concurrent and related work. Close to finishing the writing of this paper, we became aware of the very recent preprint [29], extension of the workshop paper [28], which suggests a very similar algorithm, based on a different derivation centred around optimal transport and the Fisher-Rao gradient flow; the KME-dynamics in Algorithm 1 reduces to the KFR-flow proposed in [29], if $C_t = I_{d \times d}$ and $v_t^0 \equiv 0$.

Prior work has considered Bayesian inference through kernel mean embeddings and the *kernel Bayes' rule*, see, for instance, [14, 46, 45, 44, 57] as well as [4, 32] in a slightly broader (control-theoretic) context. The kernel Bayes' rule requires a scenario slightly different from ours, in particular the availability of data from the joint parameter-observation distribution to approximate the corresponding covariance operators. Closer to our setting (where we base our inference on the negative log-likelihood h) is the *kernel Kalman rule*, see [16, 17, 51], and our approach can be viewed as a continuous-time variant tailored to the interpolation (1); see Remark 3.2 below. We would also like to point the reader to [23, Section 6], providing a discussion about Gaussian and non-Gaussian Kalman update rules for KMEs, and to [24, Section 4.1], discussing Gaussian optimal transport with quadratic kernels. Both complement our result from Proposition 3.4, stating the equivalence of KME-dynamics and the Kalman-Bucy filter for quadratic kernels. In section 4, we build on the recently introduced *kernelised diffusion maps* [37], and mention in passing that (unkernelised) diffusion maps [8] have been used in Bayesian inference following a similar line of reasoning [55, 35].

Finally, the interpolation (1) may be replaced by other reference dynamics according to the application. For example, π_t might solve the Kushner-Stratonovich SPDE from stochastic nonlinear filtering with continuous-time observations [1, Chapter 3]. Matching the mean-field dynamics (2) leads to the *feedback particle filter*, see [58, 34, 7, 54]. For a comprehensive recent overview we refer the reader to [5] and references therein.

Notation. Throughout the paper, we denote by $\mathcal{P}(\mathbb{R}^d)$ the set of probability measures on \mathbb{R}^d (equipped with the Borel σ -algebra). Probability measures and their densities with respect to the Lebesgue measure will be denoted by the same symbol. The Hilbert space of (equivalence classes of) π -square-integrable functions will be denoted by $L^2(\pi) = \{f : \mathbb{R}^d \rightarrow \mathbb{R} : \int_{\mathbb{R}^d} f^2 d\pi < \infty\}$, and the corresponding inner product by $\langle \cdot, \cdot \rangle_{L^2(\pi)}$. The space of smooth compactly supported functions on \mathbb{R}^d will be denoted by $C_c^\infty(\mathbb{R}^d)$. The set of symmetric positive definite matrices will be referred to as $\mathbb{R}_{\text{sym}, >0}^{d \times d}$. For $\rho \in \mathcal{P}(\mathbb{R}^d)$, we denote its mean by $\mu(\rho) = \int_{\mathbb{R}^d} x d\rho \in \mathbb{R}^d$, and its covariance matrix by $\text{Cov}(\rho) = \int_{\mathbb{R}^d} (x - \mu)(x - \mu)^\top d\rho \in \mathbb{R}^{d \times d}$.

2 Reproducing kernel Hilbert spaces and mean embeddings

In this section we recall relevant notions corresponding to positive definite kernels; we refer the reader to [43, 49] for background on reproducing kernel Hilbert spaces, and to [31] for a survey on kernel mean embeddings.

Positive definite kernels and feature maps. A bivariate function $k : \mathbb{R}^d \times \mathbb{R}^d \rightarrow \mathbb{R}$ is called a *positive definite kernel* if

1. it is *symmetric*, that is, $k(x, y) = k(y, x)$ for all $x, y \in \mathbb{R}^d$,
2. the corresponding Gram matrices are *positive semi-definite*, that is, for all integers $N \in \mathbb{N}$, coefficients $(\alpha_i)_{i=1}^N \subset \mathbb{R}$ and points $(x_i)_{i=1}^N \subset \mathbb{R}^d$, we have $\sum_{i,j=1}^N \alpha_i \alpha_j k(x_i, x_j) \geq 0$.

For every positive definite kernel k , there exists a unique associated *reproducing kernel Hilbert space* (RKHS), denoted $(\mathcal{H}_k, \langle \cdot, \cdot \rangle_{\mathcal{H}_k})$, characterised by the fact that $k(\cdot, x) \in \mathcal{H}_k$ for all $x \in \mathbb{R}^d$, as well as by the *reproducing property* [56, Theorem 12.11]:

$$\langle f, k(\cdot, x) \rangle_{\mathcal{H}_k} = f(x), \quad \text{for all } x \in \mathbb{R}^d, f \in \mathcal{H}_k.$$

A more constructive approach to understanding \mathcal{H}_k can be obtained as follows (see, e.g., [21, Section 2.3]): For a fixed positive definite kernel k , we may consider the *feature map*

$$\begin{aligned} \phi_k : \mathbb{R}^d &\rightarrow \mathcal{H}_k, \\ x &\mapsto k(\cdot, x), \end{aligned} \tag{4}$$

embedding the points from \mathbb{R}^d to the function space \mathcal{H}_k , typically encoding a distance-like notion between $x, y \in \mathbb{R}^d$ by $k(x, y) = \langle k(\cdot, x), k(\cdot, y) \rangle_{\mathcal{H}_k}$. Building on this intuition, the RKHS \mathcal{H}_k can be

constructed as an appropriate closure¹ of the linear span of all features:

$$\mathcal{H}_k := \overline{\left\{ f = \sum_{i=1}^N \alpha_i k(\cdot, x_i) : N \in \mathbb{N}, (\alpha_i)_{i=1}^N \subset \mathbb{R}, (x_i)_{i=1}^N \subset \mathbb{R}^d \right\}}^{\|\cdot\|_{\mathcal{H}_k}},$$

that is, \mathcal{H}_k contains (up to limits) the features $k(\cdot, x)$ that encode the points $x \in \mathbb{R}^d$.

Kernel mean embeddings. Augmenting (4), the *kernel mean embedding* (KME) [42] provides a feature map that embeds elements from the space of probability distributions into \mathcal{H}_k :

$$\begin{aligned} \Phi_k : \mathcal{P}(\mathbb{R}^d) &\rightarrow \mathcal{H}_k, \\ \rho &\mapsto \int_{\mathbb{R}^d} k(\cdot, x) \rho(dx). \end{aligned} \quad (5)$$

Clearly, Φ_k extends ϕ_k , in the sense that $\Phi_k(\delta_x) = \phi_k(x)$, where δ_x denotes the Dirac measure centred at $x \in \mathbb{R}^d$. Furthermore, expectations with respect to $\rho \in \mathcal{P}(\mathbb{R}^d)$ can be computed using the KME and the inner product in \mathcal{H}_k , that is, $\mathbb{E}_{X \sim \rho}[f(X)] = \langle f, \Phi_k(\rho) \rangle_{\mathcal{H}_k}$, for $f \in \mathcal{H}_k$, assuming that the expectation is well defined.

A natural question with particular relevance for the present paper is the extend to which $\rho \in \mathcal{P}(\mathbb{R}^d)$ can be recovered from $\Phi_k(\rho) \in \mathcal{H}_k$. The amount of information preserved by the KME depends on the chosen kernel, and kernels that allow perfect reconstruction are referred to as *characteristic* [12, 13, 47]:

Definition 2.1 (Characteristic kernels). A positive definite kernel $k : \mathbb{R}^d \times \mathbb{R}^d \rightarrow \mathbb{R}$ is called *characteristic* if and only if the corresponding KME is injective, that is, if $\Phi_k(\rho) = \Phi_k(\tilde{\rho})$ implies $\rho = \tilde{\rho}$, for all $\rho, \tilde{\rho} \in \mathcal{P}(\mathbb{R}^d)$.

According to [13], the Gaussian (or RBF) kernel

$$k(x, y) = \exp\left(-\frac{\|x - y\|^2}{2\sigma^2}\right), \quad x, y \in \mathbb{R}^d, \quad (6)$$

is characteristic. Another kernel important for the present paper is the quadratic kernel

$$k_2(x, y) := (x^\top y + 1)^2, \quad x, y \in \mathbb{R}^d, \quad (7)$$

which is closely connected to the Kalman methodology (see the Introduction) due to the following fact:

Observation 2.2 (First and second moment matching). For two probability measures $\rho, \tilde{\rho} \in \mathcal{P}(\mathbb{R}^d)$, the following are equivalent:

1. The KMEs induced by k_2 agree: $\Phi_{k_2}(\rho) = \Phi_{k_2}(\tilde{\rho})$,
2. The measures ρ and $\tilde{\rho}$ have the same mean vectors and covariance matrices.

Proof. Following [48, Example 3], this can be shown by directly computing the (squared) *maximum mean discrepancy*

$$\begin{aligned} \text{MMD}_{k_2}^2(\rho, \tilde{\rho}) &= \|\Phi_{k_2}(\rho) - \Phi_{k_2}(\tilde{\rho})\|_{\mathcal{H}_{k_2}}^2 = 2\|\mu(\rho) - \mu(\tilde{\rho})\|^2 \\ &\quad + \|\text{Cov}(\rho) - \text{Cov}(\tilde{\rho}) + \mu(\rho)\mu(\rho)^\top - \mu(\tilde{\rho})\mu(\tilde{\rho})^\top\|_F^2, \end{aligned}$$

where $\|\cdot\|_F$ denotes the Frobenius norm, and $\mu(\rho), \mu(\tilde{\rho}) \in \mathbb{R}^d$ denote the means of ρ and $\tilde{\rho}$. □

¹The closure is with respect to $\langle \cdot, \cdot \rangle_{\mathcal{H}_k} = \|\cdot\|_{\mathcal{H}_k}^2$, defined in such a way that the reproducing property (4) holds. See [21, Section 2.3] for further details.

3 RKHS embeddings for mean-field dynamics

3.1 Constructing the KME-dynamics

As alluded to in the Introduction, we consider the task of replicating the curve of tempered distributions

$$\pi_t = \frac{e^{-th}\pi_0}{Z_t}, \quad t \in [0, 1], \quad (8)$$

by the dynamics of a mean-field ordinary differential equation,

$$\frac{dX_t}{dt} = v_t(X_t) + v_t^0(X_t), \quad X_0 \sim \rho_0 = \pi_0. \quad (9)$$

We think of (9) as a parameterisation of the time-marginal distributions $\rho_t := \text{Law}(X_t)$ through the (time-dependent) vector-field v_t (possibly itself depending on ρ_t). The additional offset v_t^0 will be beneficial when prior information on the target dynamics is available, for example when the prior and the likelihood are close to Gaussian (see Section 5.3 for an example), but $v_t^0 \equiv 0$ is a viable choice. Notice that we have dropped the noise contribution from (2) by setting $\sigma_t \equiv 0$; allowing for a stochastic component is an interesting direction for future work.

Building on Section 2, we aim to match $(\rho_t)_{t \in [0, 1]}$ to $(\pi_t)_{t \in [0, 1]}$ by equating their kernel mean embeddings $(\Phi_k(\rho_t))_{t \in [0, 1]} \subset \mathcal{H}_k$ and $(\Phi_k(\pi_t))_{t \in [0, 1]} \subset \mathcal{H}_k$, for an appropriate choice of positive definite kernel $k : \mathbb{R}^d \times \mathbb{R}^d \rightarrow \mathbb{R}$. Throughout, we work under the following assumption on the compatibility between the distributions defined by (8)-(9) and the choice of kernel:

Assumption 1. *The negative log-likelihood $h : \mathbb{R}^d \rightarrow \mathbb{R}$ is measurable, and e^{-h} is π_0 -integrable. The positive definite kernel $k : \mathbb{R}^d \times \mathbb{R}^d \rightarrow \mathbb{R}$ is continuously differentiable in each argument. Furthermore, $\mathbb{R}^d \ni x \mapsto k(\cdot, x) \in \mathcal{H}_k$ is π_t -Bochner-integrable for all $t \in [0, 1]$, so that the KMEs $(\Phi_k(\pi_t))_{t \in [0, 1]}$ are well defined. Finally, we assume that $t \mapsto \Phi_k(\pi_t)$ is differentiable, for all $t \in (0, 1)$.*

Assumption 1 is relatively mild; the integrability assumptions are satisfied for instance if k has at most polynomial growth, and π_t decays exponentially at infinity. As a first step towards matching (9) to (8), we compute the evolution equations for the KMEs $\Phi_k(\pi_t)$ and $\Phi_k(\rho_t)$:

Lemma 3.1 (Evolution equations for KMEs). *The kernel mean embeddings $\Phi_k(\pi_t)$ and $\Phi_k(\rho_t)$ satisfy the \mathcal{H}_k -valued ODEs*

$$\partial_t \Phi_k(\pi_t) = -\text{Cov}_{x \sim \pi_t} [\phi_k(x), h(x)], \quad (10a)$$

$$\partial_t \Phi_k(\rho_t) = \mathbb{E}_{x \sim \rho_t} [\nabla_x \phi_k(x) \cdot (v_t + v_t^0)(x)], \quad (10b)$$

where ϕ_k denotes the feature map defined in (4), and the covariance is given by

$$\text{Cov}_{x \sim \pi_t} [\phi_k(x), h(x)] = \int_{\mathbb{R}^d} k(\cdot, x) h(x) \pi_t(dx) - \left(\int_{\mathbb{R}^d} k(\cdot, x) \pi_t(dx) \right) \left(\int_{\mathbb{R}^d} h \, d\pi_t \right).$$

Proof. Equation (10a) follows by differentiating (8) and applying the KME defined in (5). Similarly, (10b) can be obtained using the continuity equation associated to (9). Detailed calculations can be found in Appendix A.1. \square

Remark 3.2 (Kernel Bayes' and Kalman rule). A discrete-time version of (10a) reads

$$\Phi_k(\pi_{t+\Delta t}) = \Phi_k(\pi_t) - \Delta t \cdot \text{Cov}_{x \sim \pi_t} [\phi_k(x), h(x)] + \mathcal{O}(\Delta t^2), \quad (11)$$

which should be interpreted as an infinitesimal counterpart of the kernel Kalman rule [16, 17, 51], in the context where the non-negative log-likelihood h is available. It is also instructive to compare to the (uncentred) kernel Bayes' rule, see eq. (1.3) in [23].

To proceed, we equate (10a) and (10b) to obtain an integral equation for v_t :

$$-\int_{\mathbb{R}^d} \nabla_x k(\cdot, x) \cdot v_t(x) \rho_t(dx) = \underbrace{\text{Cov}_{x \sim \pi_t} [\phi_k(x), h(x)] + \mathbb{E}_{x \sim \rho_t} [\nabla_x \phi_k(x) \cdot v_t^0(x)]}_{=: f_t \in \mathcal{H}_k}, \quad (12)$$

where we have introduced the short-hand notation f_t for the right-hand side, which does not depend on v_t . Clearly, solutions to (12) will not be unique: Given a solution v_t , the modification $v_t + w_t$ will solve (12) as well, provided that w_t is orthogonal to $\nabla_x k(\cdot, x)$ in $L^2(\rho_t)$. To resolve this issue (and to obtain a symmetric form in (12), we reparameterise v_t through a scalar field $\alpha_t : \mathbb{R}^d \rightarrow \mathbb{R}$,

$$v_t(x) = -C_t \int_{\mathbb{R}^d} \nabla_x k(x, y) \alpha_t(y) \rho_t(dy), \quad (13)$$

where $C_t \in \mathbb{R}_{\text{sym}, >0}^{d \times d}$ is a (possibly time-dependent) symmetric, positive definite matrix. The point of choosing the ansatz (13) is the fact that (12) takes the form

$$\int_{\mathbb{R}^d} G_{\rho_t, C_t}(\cdot, y) \alpha_t(y) \rho_t(dy) = f_t, \quad (14)$$

as an integral equation for α_t , where we have defined the new (ρ and C -dependent) kernel

$$G_{\rho, C}(x, y) := \int_{\mathbb{R}^d} \nabla_z k(x, z) \cdot C \nabla_z k(z, y) \rho(dz), \quad (15)$$

which is positive definite (see Lemma 3.3 below) due to the judicious choice of v_t in (13). To obtain a well-posed equation for α_t (and hence for v_t), we need the following modification:

Tikhonov regularisation. Equation (14) is a prototypical example of an ill-posed inverse problem, see [22]. Indeed, since the operator $\alpha \mapsto \int_{\mathbb{R}^d} G_{\rho, C}(\cdot, y) \alpha(y) \rho(dy)$ is compact in $L^2(\rho)$, solutions to (14) need not exist, and generically will be unstable with respect to small perturbations of the right-hand side. Therefore, we will need to consider the regularised version

$$\int_{\mathbb{R}^d} G_{\rho_t, C_t}(\cdot, y) \alpha_t(y) \rho_t(dy) + \varepsilon \alpha_t = f_t, \quad (16)$$

for a small parameter $\varepsilon > 0$. In the broader context of kernel mean embeddings for Bayesian inference, the occurrence of inverse problems is not surprising; typically the solution of an integral equation is required to recover the posterior from its KME (the ‘outbedding’ or ‘pre-image’ problem; see, for instance, [17, Section 5.1.2]).

The following lemma justifies the ansatz in (13) as well as the regularisation in (16):

Lemma 3.3 (Properties of $G_{\rho, C}$). *The following holds:*

1. For $\rho \in \mathcal{P}(\mathbb{R}^d)$ and $C \in \mathbb{R}_{\text{sym}, >0}^{d \times d}$, the kernel $G_{\rho, C} : \mathbb{R}^d \times \mathbb{R}^d \rightarrow \mathbb{R}$ is symmetric and positive definite.
2. For any $\varepsilon > 0$ and $f_t \in L^2(\rho_t)$, there exists a unique solution $\alpha_t \in L^2(\rho_t)$ to (16).

Proof. See Appendix A.1. □

Combining equations (13) and (16), we obtain a two-step procedure for finding an appropriate v_t in the dynamics (9): We first solve (16) for α_t , and then compute v_t from (13). Notice that the choice of C_t is still arbitrary; in Section 3.2 below, we suggest $C_t = \text{Cov } \rho_t$, based on a comparison to the Kalman filter.

Mean-field dynamics. To close equation (16), we replace π_t by ρ_t on the right-hand side, and collect the dynamical equations and those for v_t as follows:

$$\frac{dX_t}{dt} = -C_t \int_{\mathbb{R}^d} \alpha_t(y) \nabla_{X_t} k(X_t, y) d\rho_t(y) + v_t^0(X_t), \quad X_0 \sim \rho_0, \quad (17a)$$

$$\int_{\mathbb{R}^d} G_{\rho_t, C_t}(\cdot, y) \alpha_t(y) \rho_t(dy) + \varepsilon \alpha_t = f_t, \quad (17b)$$

where the right-hand side of (17b) is given by

$$f_t = \text{Cov}_{x \sim \rho_t} [\phi_k(x), h(x)] + \mathbb{E}_{x \sim \rho_t} [\nabla_x \phi_k(x) \cdot v_t^0(x)]. \quad (18)$$

Notice that (17a) is a mean-field ODE for X_t , since the driving vector field on the right-hand side depends on the distribution $\rho_t = \text{Law}(X_t)$. In particular, α_t depends on ρ_t through (17b) since both the kernel G_{ρ_t, C_t} and the right-hand side f_t are ρ_t -dependent.

Interacting particle system. It is straightforward to translate (17) into a coupled system of ODEs for an interacting particle system $(X_t^i)_{i=1}^N \subset \mathbb{R}^d$, making the approximation $\rho_t \approx \frac{1}{N} \sum_{i=1}^N \delta_{X_t^i}$:

$$\frac{dX_t^i}{dt} = -\frac{1}{N} C_t \sum_{j=1}^N \alpha_t^j \nabla_{X_t^i} k(X_t^i, X_t^j) + v_t^0(X_t^i), \quad (19a)$$

$$\frac{1}{N} (\mathbf{G}_t + \varepsilon I_{N \times N}) \boldsymbol{\alpha}_t = \underbrace{\mathbf{h}_t^k + \mathbf{v}_t^{0,k}}_{=: \mathbf{f}_t}, \quad (19b)$$

where $\boldsymbol{\alpha}_t = (\alpha_t^1, \dots, \alpha_t^N) \in \mathbb{R}^N$ is a weight vector, $I_{N \times N} \in \mathbb{R}^{N \times N}$ refers to the identity matrix, and the entries of the matrix \mathbf{G} are given by

$$(\mathbf{G}_t)_{ij} = \frac{1}{N} \sum_{l=1}^N \nabla_{X_t^l} k(X_t^i, X_t^l) \cdot C_t \nabla_{X_t^l} k(X_t^l, X_t^j), \quad i, j = 1, \dots, N. \quad (20)$$

Note that in going from (17b) to (19b), we have also applied the rescaling $\varepsilon \mapsto \varepsilon/N$, which is harmless since ε is specified by the user. The right-hand side $\mathbf{f}_t = \mathbf{h}_t^k - \mathbf{v}_t^{0,k} \in \mathbb{R}^N$ of (19b) splits into the likelihood term

$$(\mathbf{h}_t^k)_i = \frac{1}{N} \sum_{j=1}^N k(X_t^i, X_t^j) h(X_t^j) - \left(\frac{1}{N} \sum_{j=1}^N h(X_t^j) \right) \left(\frac{1}{N} \sum_{l=1}^N k(X_t^i, X_t^l) \right), \quad i = 1, \dots, N, \quad (21)$$

and the correction term

$$(\mathbf{v}_t^{0,k})_i = \frac{1}{N} \sum_{j=1}^N \nabla_{X_t^j} k(X_t^i, X_t^j) \cdot v_t^0(X_t^j). \quad (22)$$

We expect the dynamics of (19) to be close to those of (17) in an appropriate sense, but a rigorous proof is beyond the scope of the current paper. Discretising (19) in time using the Euler scheme leads to Algorithm 1, summarising the KME-dynamics approach to Bayesian inference.

Algorithm 1 KME-dynamics

Require: samples $(X_0^i)_{i=1}^N$ from π_0 , negative log-likelihood $h : \mathbb{R}^d \rightarrow \mathbb{R}$, baseline vector field v_t^0 , positive definite kernel $k : \mathbb{R}^d \times \mathbb{R}^d \rightarrow \mathbb{R}$, number of steps N_{steps} , time-dependent matrix $C_t \in \mathbb{R}_{\text{sym}, >0}^{d \times d}$, regularisation parameter ε .

Output: approximate samples $(X_1^i)_{i=1}^N$ from π_1 .

- 1: Set the step size $\Delta t \leftarrow 1/N_{\text{steps}}$.
- 2: **for** $n = 0, \dots, N_{\text{steps}} - 1$ **do**
- 3: Compute $\mathbf{G}_{n\Delta t}$, $\mathbf{h}_{n\Delta t}^k$ and $\mathbf{v}_{n\Delta t}^{0,k}$ using (20), (21) and (22).
- 4: Solve the linear system (19b) for $\boldsymbol{\alpha}_{n\Delta t}$.
- 5: **for** $i = 1, \dots, N$ **do**
- 6: $X_{(n+1)\Delta t}^i \leftarrow X_{n\Delta t}^i - \frac{\Delta t}{N} \cdot C_{n\Delta t} \sum_{j=1}^N \alpha_{n\Delta t}^j \nabla_{X_{n\Delta t}^i} k(X_{n\Delta t}^i, X_{n\Delta t}^j) + \Delta t \cdot v_{n\Delta t}^0(X_{n\Delta t}^i)$.
- 7: **end for**
- 8: **end for**

3.2 Quadratic kernels and the Kalman update

In this section, we discuss the particular case when the Bayesian prior and the likelihood are both Gaussian,

$$\pi_0 = \mathcal{N}(\mu_0, \Sigma_0), \quad h(x) = \frac{1}{2}(Hx - \beta) \cdot R^{-1}(Hx - \beta), \quad (23)$$

with prior mean $\mu_0 \in \mathbb{R}^d$ and prior covariance $\Sigma_0 \in \mathbb{R}^{d \times d}$, observation $\beta \in \mathbb{R}^{d'}$, observation operator $H \in \mathbb{R}^{d' \times d}$ and observation noise covariance $R \in \mathbb{R}^{d' \times d'}$, see, for example, [40, Section 6.1]. In this scenario, the posterior π_1 remains Gaussian, with mean and covariance available in closed form. As shown in [2, 3, 39], the Bayesian update can be implemented in an algorithmically robust way via the mean field Kalman-Bucy ODE

$$\frac{dX_t}{dt} = -\frac{1}{2} \text{Cov}(\rho_t) H^\top R^{-1} (HX_t + \mu(\rho_t) - 2\beta), \quad X_0 \sim \pi_0, \quad (24)$$

that is, the solution to (24) satisfies $X_1 \sim \pi_1$. In (24), we use $\rho_t = \text{Law}(X_t)$ for the associated distribution, and $\mu(\rho_t)$ for the corresponding mean.

As suggested by Observation 2.2 and the construction in Section 3.1 based on (3), there should be a close connection between the KME-dynamics (17) and the Kalman-Bucy ODE (24) for the quadratic kernel k_2 defined in (7). The following result shows that indeed the KME-dynamics (17) reduces to (24) if we set C_t to be the covariance matrix of ρ_t .

Proposition 3.4 (From KME-dynamics to Kalman-Bucy). *Assume that π_0 and h are given by (23), hence π_t are Gaussian for all $t \in [0, 1]$, and furthermore that*

$$k(x, y) = (x^\top y + 1)^2, \quad C_t = \text{Cov}(\rho_t). \quad (25)$$

Then the evolution equations (17) and (24), and hence their solutions, coincide, as $\varepsilon \rightarrow 0$.

Proof. The proof proceeds by direct (although somewhat lengthy) calculation, see Appendix A.1. \square

Remark 3.5. It is worth stressing that the relationship between the KME and Kalman-Bucy dynamics does not extend to the respective interacting particle systems (given by (19) for the KME-dynamics and by replacing the mean and covariance in (24) by their estimator versions). Indeed, the proof of Proposition 3.4 rests on identities between higher-order moments of Gaussian measures (see Lemma A.1), which are satisfied only approximately for the empirical measures. A more fine-grained exploration of the finite-sample properties of the KME-dynamics is left for future work.

Based on Proposition 3.4 and the well-documented good performance of Kalman-type methods, we suggest implementing the KME interacting particle system (19) with the choice

$$C_t = \frac{1}{N-1} \sum_{i=1}^N (X_t^i - \bar{X}_t)(X_t^i - \bar{X}_t)^\top, \quad (26)$$

the empirical covariance matrix for the ensemble $(X_t^i)_{i=1}^n$. In settings with Gaussian likelihood, it is reasonable to use (24) as a baseline dynamics; we hence advertise

$$v_t^0(x) = v_{\text{Kalman}}(x) := -\frac{1}{2} \text{Cov}(\rho_t) H^\top R^{-1} (Hx + \mu(\rho_t) - 2\beta) \quad (27)$$

and evaluate its empirical performance in Section 5.3.

Remark 3.6 (Affine invariance). The choice $C_t = \text{Cov}(\rho_t)$ is not sufficient to make the KME-dynamics (17) affine-invariant in the sense of [18, 6, 15]; this would require appropriate scaling of the kernel k .

4 Variational formulation and kernelised diffusion maps

In this section, we provide further insight into the KME mean-field dynamics (17) by giving a variational principle for the vector field on the right-hand side of (17a). For simplicity, we will only consider the case $v_t^0 \equiv 0$. To set the stage, we define the norm

$$\|v\|_{(L^2(\rho))^d, C}^2 := \int_{\mathbb{R}^d} v \cdot C^{-1} v \, d\rho \quad (28)$$

on $(L^2(\rho))^d$, where $C \in \mathbb{R}^{d \times d}$ is a fixed symmetric positive definite matrix. We also recall the *maximum mean discrepancy*

$$\text{MMD}_k^2(\rho, \tilde{\rho}) := \|\Phi_k(\rho) - \Phi_k(\tilde{\rho})\|_{\mathcal{H}_k}^2 \quad (29)$$

between two signed measures ρ and $\tilde{\rho}$, see [31, Section 3.5], which should be interpreted as measuring the distance between ρ and $\tilde{\rho}$ through the embedding Φ_k and the RKHS-norm $\|\cdot\|_{\mathcal{H}_k}^2$. In the following result, we interpret the ODE $\frac{dX_t}{dt} = v_t(X_t)$ as giving rise to the signed measure $\partial_t \rho_t^v$: The change of the density describing the law of X_t is induced by the vector field v , and we have $\partial_t \rho_t^v = -\nabla \cdot (\rho_t^v v)$ according to the continuity equation.²

Proposition 4.1. *Assume that $k : \mathbb{R}^d \times \mathbb{R}^d \rightarrow \mathbb{R}$ is bounded and twice continuously differentiable, with bounded derivatives. Fix $\varepsilon > 0$ and $t \in (0, 1)$, and assume that $\rho_t \in \mathcal{P}(\mathbb{R}^d)$ admits a continuously differentiable density with respect to the Lebesgue measure (so that $\partial_t \rho_t^v = -\nabla \cdot (\rho_t^v v)$ can be interpreted as a signed measure, for smooth v). Then the functional*

$$J_{\varepsilon, t}(v) := \text{MMD}_k^2(\partial_t \rho_t^v, \partial_t \pi_t) + \varepsilon \|v\|_{L^2(\rho_t), C}^2 \quad (30)$$

admits a unique minimiser $v^* \in (L^2(\rho))^d$ which coincides with the right-hand side of (17); for

$$v^* = -C_t \nabla \int_{\mathbb{R}^d} \alpha_t(y) k(\cdot, y) d\rho_t(y), \quad (31)$$

with α_t solving (17b), we have that $J_{\varepsilon, t}(v^*) \leq J_{\varepsilon, t}(v)$, for all $v \in (L^2(\rho_t))^d$.

Proof. See Appendix A.3. The proof gives a regularised regression type interpretation to (30) and identifies (17) as the corresponding normal equations. \square

Remark 4.2 (Discrete-time interpretation). Assuming perfect matching $\rho_t = \pi_t$ at fixed $t \in (0, 1)$, and approximating $\partial_t \rho_t^v \approx \frac{1}{\Delta t} (\rho_{t+\Delta t}^v - \rho_t^v)$ and $\partial_t \pi_t \approx \frac{1}{\Delta t} (\pi_{t+\Delta t} - \pi_t)$, the functional (30) takes the form

$$J_{\varepsilon, t}(v) \approx \frac{1}{\Delta t^2} \text{MMD}_k^2(\rho_{t+\Delta t}^v, \pi_{t+\Delta t}) + \varepsilon \|v\|_{L^2(\rho_t), C}^2. \quad (32)$$

Therefore, the KME-dynamics (17) can be thought of as matching $(\rho_t)_{t \in [0, 1]}$ to $(\pi_t)_{t \in [0, 1]}$ according to maximum mean discrepancy, with an L^2 -regularisation on the velocity. It is worth pointing out that similar variational formulations are available for the Kalman-Bucy vector field (27), see [41, Section 3.6], and for the conditional mean embedding in the kernel Bayes' rule [19].

The Poisson equation and infinitesimal generators of diffusions. In the remainder of this section, we connect the variational formulation from Proposition 4.1 to other related work, in particular to the kernelised diffusion maps introduced in [37]. We start by recalling a fundamental connection between the interpolation (8) and second-order elliptic operators:

To any symmetric positive definite matrix $C \in \mathbb{R}_{\text{sym}, >0}^{d \times d}$ and probability measure $\pi \in \mathcal{P}(\mathbb{R}^d)$ with strictly positive and differentiable Lebesgue density, we associate the operator

$$\mathcal{L}_{\pi, C} \phi = \frac{1}{\pi} \nabla \cdot (\pi C \nabla \phi), \quad \phi \in C_c^\infty, \quad (33)$$

extended to an unbounded operator acting on $L^2(\pi)$. It is straightforward to check that $-\mathcal{L}_{\pi, C}$ is positive semi-definite and self-adjoint, and we furthermore assume that $\mathcal{L}_{\pi, C}$ admits a spectral gap (see [36, Chapter 4] for an in-depth discussion).

Remark 4.3. We may allow C to be position dependent (also in (17) and (19)), but will not pursue this direction in this paper. The operator $\mathcal{L}_{\pi, C}$ is the infinitesimal generator of the diffusion

$$dX_t = C(X_t) \nabla \log \pi(X_t) dt + (\nabla \cdot C)(X_t) dt + \sqrt{2C(X_t)} dW_t, \quad (34)$$

see [36, Section 2.3], which may be interpreted as overdamped Langevin diffusion on a Riemannian manifold with metric tensor C^{-1} ; see, for instance, [27].

²Notice that ρ_t^v and v need to be regular enough so that $-\nabla \cdot (\rho_t^v v)$ can be interpreted as a signed measure.

The following is a well-known result: In order to match the interpolation (8), it is sufficient to solve linear elliptic PDEs involving $\mathcal{L}_{\pi,C}$ and h .

Lemma 4.4 (The Poisson equation for replicating mean-field dynamics). *Assume that $\phi \in C^2([0, 1] \times \mathbb{R}^d; \mathbb{R})$ solves the Poisson equation*

$$-\mathcal{L}_{\pi_t, C_t} \phi_t = h - \int_{\mathbb{R}^d} h \, d\pi_t, \quad (35)$$

for all $t \in [0, 1]$, and that the mean-field ODE

$$\frac{dX_t}{dt} = -C_t \nabla \phi_t(X_t), \quad X_0 \sim \pi_0 \quad (36)$$

admits a unique solution. Then the law of X_t reproduces the interpolation $(\pi_t)_{t \in [0, 1]}$, that is, $\text{Law}(X_t) = \pi_t$, for all $t \in [0, 1]$.

Proof. The proof can for instance be found in [39] or [20], and proceeds by differentiating (8) and using the continuity equation for (36). \square

In [28, 29], the authors recently derived the KME-dynamics (17) (with $C_t = I_{N \times N}$ and $v_t^0 = 0$) starting from the Poisson equation (35) and assuming that $\phi \in \mathcal{H}_k$. In what follows, we summarise a related approach that connects directly to the formulation in (30).

Kernelising $\mathcal{L}_{\pi,C}$. In keeping with the general construction principle from Section 3.1, and motivated by Lemma 4.4, it is plausible to ‘embed’ the operator $\mathcal{L}_{\pi,C}$ into an RKHS, and solve an embedded version of the Poisson equation (35). To this end, assume that the positive definite kernel k is bounded, with bounded first and second order derivatives, $k \in C_b^2(\mathbb{R}^d \times \mathbb{R}^d; \mathbb{R})$. Under these conditions, \mathcal{H}_k is continuously embedded in $L^2(\pi)$, see [49, Theorem 4.26], and we denote the canonical inclusion by $i : \mathcal{H}_k \hookrightarrow L^2(\pi)$.³ Following the same reference, the adjoint $i^* : L^2(\pi) \rightarrow \mathcal{H}_k$, characterised by

$$\langle f, ig \rangle_{L^2(\pi)} = \langle i^* f, g \rangle_{\mathcal{H}_k}, \quad \text{for all } f \in L^2(\pi), g \in \mathcal{H}_k,$$

is given by the integral operator

$$i^* f = \int_{\mathbb{R}^d} k(\cdot, x) f(x) \pi(dx). \quad (37)$$

Following [37], we define the *kernelisation* of $\mathcal{L}_{\pi,C}$ by

$$\mathcal{L}_{\pi,C}^k := i^* \mathcal{L}_{\pi,C} i. \quad (38)$$

The operator $\mathcal{L}_{\pi,C}^k$ acts on \mathcal{H}_k and is self-adjoint, since $\mathcal{L}_{\pi,C}$ is self-adjoint in $(L^2(\pi), \langle \cdot, \cdot \rangle_{L^2(\pi)})$, see [36, Section 4.6]. The following key lemma, due to [37, Proposition 3], shows that the inverse of $\mathcal{L}_{\pi,C}$ (and hence solutions to the Poisson equation (35)) can be obtained from the inverse of its kernelisation $\mathcal{L}_{\pi,C}^k$.

Lemma 4.5 ([37], Proposition 3.3). *Assuming that $k \in C_b^2(\mathbb{R}^d \times \mathbb{R}^d; \mathbb{R})$ and that $\mathcal{L}_{\pi,C}$ admits an $L^2(\pi)$ -spectral gap, we have that*

$$\mathcal{L}_{\pi,C}^{-1} = i(\mathcal{L}_{\pi,C}^k)^{-1} i^*, \quad (39)$$

where the (39) holds on the centred Sobolev space $H_0^1(\pi) = \left\{ f \in L^2(\pi) : \int_{\mathbb{R}^d} \|\nabla f\|^2 < \infty, \int_{\mathbb{R}^d} f \, d\pi = 0 \right\}$.

Combining Lemma 4.4 and Lemma 4.5, we see that an appropriate vector field can be obtained by setting

$$v_t = -C_t \nabla i(\mathcal{L}_{\pi,C}^k)^{-1} i^* \bar{h}_t, \quad (40)$$

with the shorthand notation $\bar{h}_t = h - \int_{\mathbb{R}^d} h \, d\pi_t$. Comparing (40) and (31), we see that the kernelised diffusion map approach recovers the KME vector field, using the calculations in [37, Section 3] to obtain a closed-form expression for $\mathcal{L}_{\pi,C}^k$. Indeed, $i^* \bar{h}_t$ corresponds to the right-hand side in (17b), for

³This inclusion is essentially the identity, $i(f) = f$. However, note that $f \in \mathcal{H}_k$ is indeed a function, whereas $i(f) \in L^2(\pi)$ is an equivalence class (under equality up to a π -null set).

$v_t^0 = 0$, and $\mathcal{L}_{\pi,C}^k$ implements the integral operator on the left-hand side.

Regression interpretation. Let us introduce the scaled gradient operator $A := C\nabla$, viewed as acting between function spaces as $A : L^2(\pi) \rightarrow (L^2(\pi))^d$. It is straightforward to verify that its adjoint with respect to $\langle \cdot, \cdot \rangle_{(L^2(\pi))^d, C}$ is given by $A^*v = -\frac{1}{\pi}\nabla \cdot (\pi v)$. Indeed,

$$\langle v, A\phi \rangle_{(L^2(\pi))^d, C} = \langle A^*v, \phi \rangle_{L^2(\pi)}, \quad \text{for all } \phi \in L^2(\pi), v \in (L^2(\pi))^d. \quad (41)$$

Therefore, we can write $\mathcal{L}_{\pi,C} = -A^*A$, and, using (40), we can express the KME vector field (31) as

$$v^* = Ai(i^*A^*Ai + \varepsilon)^{-1}i^*\bar{h} \quad (42a)$$

$$= Ai((Ai)^*(Ai) + \varepsilon)^{-1}i^*\bar{h}, \quad (42b)$$

where we have dropped the time-indices for notational efficiency, but note that the adjoints depend on time through the underlying measure π_t . We would also like to stress that in (42a), we have $i^* : L^2(\pi) \rightarrow \mathcal{H}_k$ and $A^* : (L^2(\pi))^d \rightarrow L^2(\pi)$, that is, the adjoints are taken with respect to different spaces and inner products (implied by the domains and target spaces of i and A). Inspection of (42b) shows that v^* is obtained from a normal-form expression for a regularised regression-type problem of the form

$$(Ai)^*v = i^*\bar{h}, \quad (43)$$

see [22, Section 2.2]. More specifically, v^* minimises an appropriate Tikhonov functional which turns out to be equivalent to (30). For details, we refer to the proof of Proposition 4.1 in Appendix A.3.

5 Numerical experiments

In this section, we evaluate the KME-dynamics from Algorithm 1 through toy and filtering experiments, and demonstrate its performance as the dimension d of the underlying space increases.

In our experiments, we employ two positive definite kernel functions: the quadratic kernel, as defined in (7), and the Gaussian characteristic kernel (6), also called radial basis function (RBF) kernel. To improve reproducibility, we generate samples for Gaussian prior distributions by creating a uniformly distributed Sobol sequence (using the *Sobol* Julia package), which is then transformed into normally distributed pseudo-random numbers using the Gaussian inverse c.d.f.. Furthermore, recall that the time-dependent matrix C_t is chosen as the ensemble covariance matrix at each iteration, see (26).

5.1 Toy examples

We test the KME-dynamics with three 1-dimensional toy examples. All of these three experiments are tested with ensemble size $N = 500$, number of time steps $N_{\text{steps}} = 50$, and baseline vector field $v_t^0 \equiv 0$, for all $t \in [0, 1]$.

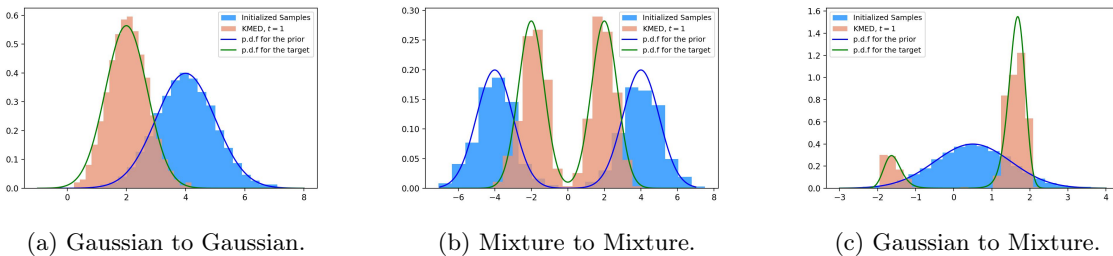


Figure 1: Three toy examples.

- **Gaussian to Gaussian.** In this case, we define the negative log-likelihood to be $h(x) = \frac{1}{2}x^2$, and initialise samples from $\pi_0 = \mathcal{N}(4, 1)$. A straightforward computation shows that the target posterior is given by $\mathcal{N}(2, 0.5)$. We apply the RBF kernel with bandwidth $\sigma = 5$, and fix the regularisation as $\varepsilon = 10^{-9}$.

- **Mixture to Mixture.** In this case we define the negative log-likelihood to be $h(x) = \frac{1}{2}x^2$, and initialise samples from $\pi_0 = \frac{1}{2}\mathcal{N}(4, 1) + \frac{1}{2}\mathcal{N}(-4, 1)$. A straightforward computation shows that the target is $\frac{1}{2}\mathcal{N}(2, 0.5) + \frac{1}{2}\mathcal{N}(-2, 0.5)$. Again, we apply the RBF kernel with bandwidth of $\sigma = 5$, and fix the regularisation as $\varepsilon = 10^{-9}$.
- **Gaussian to Mixture.** In this case we define the negative log-likelihood to be $h(x) = (3 - x^2)^2$, and initialise samples from $\pi_0 = \mathcal{N}(0.5, 1)$. We compute the p.d.f for the target as $\pi_1(x) = \frac{e^{-h(x)}\pi_0(x)}{Z}$, where the normalizing constant $Z = \int_{-\infty}^{\infty} e^{-h(x)}\pi_0(x)dx$ is computed numerically using the Julia package *QuadGK*. We apply the RBF kernel with bandwidth $\sigma = 0.95$, and fix the regularisation as $\varepsilon = 10^{-8}$.

The results of the toy experiments are visualised in Figure 1, where we plot the normalised histograms for X_0 and X_1 , and compare them to the exact p.d.f.’s for the priors and targets. Figure 1 shows that the KME-Dynamics can produce high-quality samples, although some challenges remain in the ‘Gaussian to Mixture’ (splitting of probability mass) example. We conjecture that including a noise term as in (2) might mitigate this problem, and leave further exploration for future work.

5.2 Kernel choice

In this section, we explore the question of kernel choice for the KME-dynamics; in particular, we contrast the performance of the quadratic Kalman-like kernel (7) with the characteristic RBF kernel (6).

One-dimensional skew-normal target. Here, we choose $\pi_0 = \mathcal{N}(0, 1)$ as the prior and $h(x) = -\log(2\Phi(-2x))$ as the negative log-likelihood, where Φ is the Gaussian c.d.f.. In Figure 2, we show normalised histograms of the posterior approximation, obtained by the KME-dynamics with RBF-kernel (Figure 2a) and quadratic kernel (Figure 2b), both of them with parameters $N = 200$, $N_{\text{steps}} = 50$, $v_t^0 = 0, \forall t$, and $\varepsilon = 10^{-8}$. Comparing with the target p.d.f., we see that the RBF kernel outperforms the quadratic kernel in this case, capturing the nonlinearity in the dynamical evolution. As suggested by Observation 2.2 and Proposition 3.4, the quadratic kernel provides a Gaussian approximation.

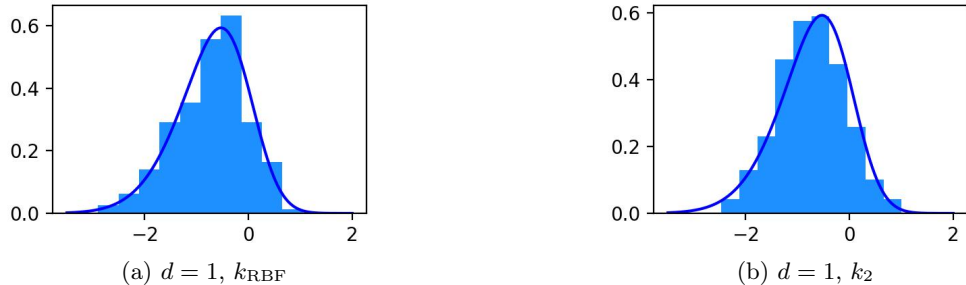
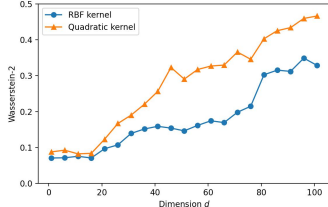
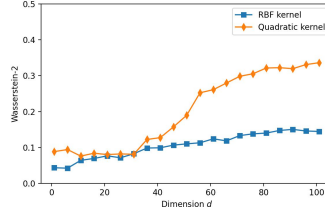


Figure 2: Posterior approximation and target p.d.f. for the one-dimensional skew-normal experiment.

High dimensional skew-normal target. Generalising the previous experiment to higher dimensions, we choose $\pi_0 = \mathcal{N}(0, I_{d \times d})$ as the prior and $h(x) = -\log(2\Phi(\gamma^\top x))$ as the negative log-likelihood, where $\gamma^\top = [-2, 0, 0, \dots, 0]$. In Figure 3 we plot the Wasserstein-2 distance [11] between the first component of the posteriors and the true target (1d skew-normal), against the dimension d (using the Julia package *OptimalTransport*). We choose either $N = 200$ particles (Figure 3a), or $N = 500$ particles (Figure 3b) are examined. The KME-Dynamics are performed with both the RBF-kernel and the quadratic kernel, each with parameters $N_{\text{steps}} = 50$, $v_t^0 = 0, \forall t$, and $\varepsilon = 10^{-8}$. As expected, the performance of KME-Dynamics get worse when the dimensionality of the space grows, and improves with more samples. Notably, the RBF kernel always outperforms the quadratic kernel. In particular, the characteristic (nonparametric) RBF kernel appears to work significantly better when the dimension is greater than 20, and when the number of particles is fairly large.



(a) $N = 200$ particles.



(b) $N = 500$ particles.

Figure 3: Wasserstein-2 distances between the approximate posteriors obtained by the KME-Dynamics and the true target (for the first marginal) versus dimension. Samples size compared for $N = 200$ (left) and $N = 500$ (right).

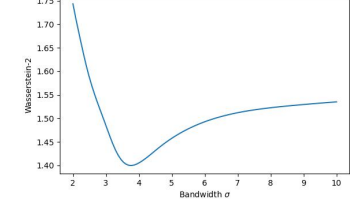


Figure 4: Wasserstein-2 distances between the posteriors and the true target versus the bandwidth of the RBF kernel.

Choice of bandwidth; overfitting and underfitting. From the perspective of the embedding (3), we suspect that \mathcal{H} should neither be too small nor too large for optimal performance of the KME-dynamics: Indeed, if \mathcal{H} is too small, then the embedding Φ is not very expressive, and the accuracy in reproducing $(\pi_t)_{t \in [0,1]}$ is low (overfitting). If \mathcal{H} is excessively large, we might expect fragile behaviour when the size of the ensemble is moderate (underfitting).

To investigate this conjecture, we study the effect of choosing different bandwidths for the RBF-kernel (6): For two bandwidths $\sigma_2 \geq \sigma_1 > 0$, we have $\mathcal{H}_{k_{\sigma_2}} \subset \mathcal{H}_{k_{\sigma_1}}$, see [49, Proposition 4.46], and thus we expect there to be an intermediate optimal choice for σ , trading of bias and variance. In our experiment, we choose $\pi_0 = \mathcal{N}((1, 1, \dots, 1, 1)^\top, I_{10 \times 10})$ as 10-dimensional Gaussian prior, and $h(x) = \frac{1}{2}x^\top x$ as the negative log-likelihood, yielding the target posterior $\pi_1 = \mathcal{N}((\frac{1}{2}, \dots, \frac{1}{2})^\top, \frac{1}{2}I_{10 \times 10})$. We perform KME-Dynamics with RBF kernel, with parameters $N = 250$, $d = 10$, $N_{\text{steps}} = 50$, $\varepsilon = 10^{-5}$, and $v_t^0 = 0$ for all $t \in [0, 1]$. In Figure 4 we plot the Wasserstein-2 distances between the approximate posteriors and the target against the bandwidth of the RBF kernel. As expected, the KME-Dynamics with RBF kernel is optimized by a specific choice of bandwidth, to prevent from overfitting or underfitting.

5.3 Data assimilation in Lorenz-63

In this section we compare the KME-Dynamics with the Ensemble Kalman Filter (EnKF) in the context of the nonlinear filtering problem for the Lorenz-63 system, which is studied in detail in [40]. Similar experiments were conducted by Stordal et al. [50], who compared the EnKF to the mapping particle filter [38], another kernel-based method that rests on Stein variational gradient descent (SVGD) [26].

We first explain the basic framework of this experiment. The evolution of the Lorenz-63 system is defined by three ODEs:

$$\frac{dx_t}{dt} = 10(y_t - x_t), \quad \frac{dy_t}{dt} = x_t(28 - z_t) - y_t, \quad \frac{dz_t}{dt} = x_t y_t - \frac{8}{3}z_t, \quad (44)$$

where (x_t, y_t, z_t) is a curve in \mathbb{R}^3 .

In the following experiments, we will go through the following procedure:

- 1. Create observations:** We integrate (44) using the the 4th-order Runge-Kutta method with time step $\delta t = 0.001$, starting from the initial condition $(x_0, y_0, z_0) = (-0.587, -0.563, 16.870)$. We set the observation time window to $\Delta t = 0.05$, and collect noisy observations

$$\beta_j = (x_{t_j}, y_{t_j}, z_{t_j}) + \xi_j, \quad (45)$$

at times $t_j = j\Delta t$, for $j = 1, \dots, 100$. In (45), the perturbations are iid normally distributed, $\xi_j \sim \mathcal{N}(0, 0.2I_{3 \times 3})$.

2. **Filter:** We sample N ensemble members $(X_0^i)_{i=1}^N$ from the Gaussian initial prior $\mathcal{N}(\mu_0, \Sigma_0)$, with mean $\mu_0 = (-0.587, -0.563, 16.870)$ and covariance $\Sigma_0 = 0.01I_{3 \times 3}$. For $j = 0, \dots, 99$, we repeat the following steps:

- *Forecast:* In the interval $[j\Delta t, (j+1)\Delta t]$, every ensemble member is propagated using a noisy version of 4-th order Runge-Kutta for (44); at every step, the positions are perturbed by iid Gaussian noise with distribution $\mathcal{N}(0, \frac{4\delta t}{5}I_{3 \times 3})$.
- *Inference:* At time $t_j = j\Delta t$, the ensemble $(X_{j\Delta t}^i)_{i=1}^N$ is regarded as samples from the prior π_0 , and we perform Bayesian inference (using either KME-dynamics or the EnKF) with negative log-likelihood $h_j(x) = \frac{5}{2}(x - \beta_j)^\top(x - \beta_j)$, that is, the observation covariance is $R = \frac{1}{5}I_{3 \times 3}$.

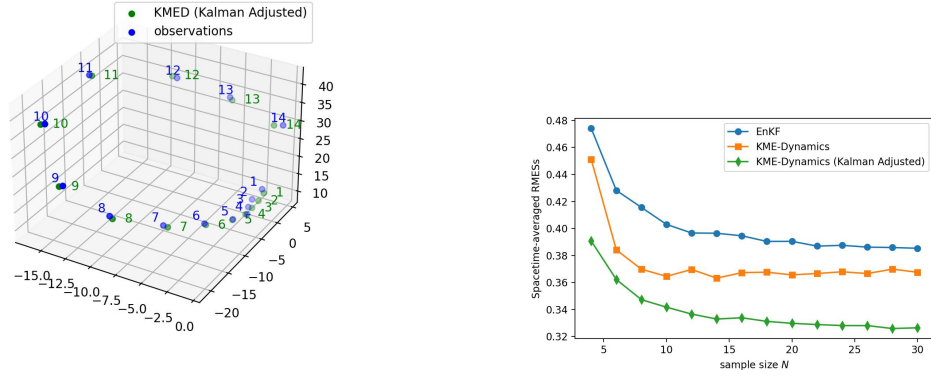


Figure 5: An example of assimilation in Lorentz-63 is shown on the left, where we plotted the first 14-th assimilations. A comparison between three filtering methods is shown on the right, where we plot the spacetime-averaged RMSEs against samples sizes for three methods, respectively.

We compare three methods for the inference step: Firstly, the Ensemble Kalman Filter (EnKF) is implemented as in [40, Algorithm 7.7]. Secondly, we use the KME-Dynamics with $N_{\text{steps}} = 50$, $v_t^0 \equiv 0$, $\forall t \in [0, 1]$, $\varepsilon = 5 \times 10^{-11}$, and RBF kernel with bandwidth $\sigma = 6$. Thirdly, we test the Kalman Adjusted KME-Dynamics by taking the KME-Dynamics with Kalman-Bucy velocity (27) as the baseline v_t^0 (all other parameters are set as before).

Figure 5a showcases observations and posterior means obtained by the Kalman-adjusted KME-dynamics for $N = 500$ particles. We denote by $(\bar{x}_j, \bar{y}_j, \bar{z}_j)$ the approximate posterior means, and plot in Figure 5b the spacetime-averaged root mean-square error (RMSE)

$$\frac{1}{3} \left(\sqrt{\frac{1}{100} \sum_{j=1}^{100} (\bar{x}_j - \beta_j^x)^2} + \sqrt{\frac{1}{100} \sum_{j=1}^{100} (\bar{y}_j - \beta_j^y)^2} + \sqrt{\frac{1}{100} \sum_{j=1}^{100} (\bar{z}_j - \beta_j^z)^2} \right),$$

averaged over 20 runs, against the number of particles. The unadjusted KME-dynamics proved slightly unstable for small ensemble sizes; those runs were discarded and repeated.

As expected, the performance of all methods improves with larger sample sizes. In this experiment, with suitable choice of bandwidth, the KME-Dynamics (with characteristic kernel) can outperform the EnKF. It is slightly surprising that the advantage of the KME-dynamics (a nonparametric method) over the EnKF diminishes with increasing ensemble size. We conjecture that this is due to errors in the linear inversion (19b), and that better results might be obtained with a sophisticated tuning schedule of the regularisation. Remarkably, the hybrid Kalman-adjusted KME-dynamics appears to considerably reduce the RMSE.

6 Discussion and Outlook

We have developed KME-dynamics as an algorithmic approach for general Bayesian inference, which does not require the score of the target posterior, and is therefore applicable to settings in data assimilation. Based on kernel mean embeddings, KME-dynamics captures statistical information in reproducing kernel Hilbert spaces, and moves the ensemble members in an interacting particle system accordingly. The framework seamlessly accommodates the Kalman-Bucy filter, as well as a predefined baseline dynamics. The latter modification has shown particular promise in our numerical experiment for the Lorenz-63 system, combining a Kalman update with a nonlinear refinement. Across all our experiments, we have observed benefits from choosing a characteristic kernel, incorporating information through the KME in a lossless manner.

In future work, we plan to build on the exposed connection between KME-dynamics, kernelised diffusion maps and Tikhonov functionals, leveraging insights from statistical learning theory to improve both the implementation of KME-dynamics as well as its theoretical understanding. It is also of interest to clarify the connection of the KME-dynamics to Stein variational gradient descent [26], and to its geometrical underpinnings [9, 33]. Finally, it may be interesting to consider more general interpolations than (1), in the spirit of [53, 52].

A Proofs and calculations

A.1 Proofs for Section 3.1

Proof of Lemma 3.1. For (10a), we begin by computing the time derivative of the normalising constant,

$$\partial_t Z_t = \partial_t \int_{\mathbb{R}^d} e^{-th} d\pi_0 = - \int_{\mathbb{R}^d} h e^{-th} d\pi_0 = -Z_t \int_{\mathbb{R}^d} h d\pi_t. \quad (46)$$

Using this, we see that

$$\partial_t \pi_t = -h\pi_t - \frac{\partial_t Z_t e^{-th} \pi_0}{Z_t^2} = -h\pi_t + \pi_t \int_{\mathbb{R}^d} h d\pi_t. \quad (47)$$

For the kernel mean embedding, we therefore obtain

$$\partial_t \Phi_k(\pi_t) = \int_{\mathbb{R}^d} k(\cdot, x) \partial_t \pi_t(dx) = - \int_{\mathbb{R}^d} k(\cdot, x) \left(h(x) - \int_{\mathbb{R}^d} h d\pi_t \right) \pi_t(dx), \quad (48)$$

which can be rewritten in the form (10a).

For (10b), notice that the continuity equation associated to (9) reads

$$\partial_t \rho_t + \nabla \cdot (\rho_t(v_t + v_t^0)) = 0. \quad (49)$$

For the kernel mean embedding, we thus obtain

$$\partial_t \Phi_k(\rho_t) = - \int_{\mathbb{R}^d} k(\cdot, x) \nabla_x \cdot (\rho_t(v_t + v_t^0))(x) dx = \int_{\mathbb{R}^d} \nabla_x k(\cdot, x) \cdot (v_t + v_t^0)(x) dx, \quad (50a)$$

as required. \square

Proof of Lemma 3.3. 1.) Clearly, $G_{\rho, C}$ is symmetric, by the symmetry of C . To check positive definiteness, we fix $N \in \mathbb{N}$, choose $(\alpha_i)_{i=1}^N \subset \mathbb{R}$ and $(x_i)_{i=1}^N \subset \mathbb{R}^d$, and notice that

$$\begin{aligned} \sum_{i,j=1}^N \alpha_i \alpha_j G_{\rho, C}(x_i, x_j) &= \int_{\mathbb{R}^d} \left(\sum_{i=1}^N \alpha_i \nabla_z k(x_i, z) \right) \cdot C \left(\sum_{i=1}^N \alpha_i \nabla_z k(x_i, z) \right) \rho(dz) \\ &= \int_{\mathbb{R}^d} \left| C^{1/2} \sum_{i=1}^N \alpha_i \nabla_z k(x_i, z) \right|^2 \rho(dz) \geq 0 \end{aligned}$$

2.) This follows from the general theory of regularised inverse problems, see, for example [22, Section 2.2]. \square

A.2 Proof of Proposition 3.4

We will need the following lemma, see, for instance [30].

Lemma A.1 (Gaussian moments). *For a Gaussian random variable $X \sim \mathcal{N}(\mu, \Sigma)$ in \mathbb{R}^d , denote $\Omega_{ij} := \mu_i \mu_j$. Then we have the following expressions for the moments:*

$$\mathbb{E}[X_i] = \mu_i, \quad \mathbb{E}[X_i X_j] = \Sigma_{ij} + \Omega_{ij}, \quad (51a)$$

$$\mathbb{E}[X_i X_j X_k] = \mu_i \Sigma_{jk} + \mu_j \Sigma_{ik} + \mu_k \Sigma_{ij} + \Omega_{ij} \mu_k, \quad (51b)$$

$$\mathbb{E}[X_i X_j X_k X_l] = \Sigma_{ij} \Sigma_{kl} + \Sigma_{ik} \Sigma_{jl} + \Sigma_{il} \Sigma_{jk} + \Omega_{ij} \Sigma_{kl} + \Omega_{ik} \Sigma_{jl} + \Omega_{il} \Sigma_{jk} + \Omega_{jk} \Sigma_{il} + \Omega_{jl} \Sigma_{ik} + \Omega_{kl} \Sigma_{ij} + \Omega_{ij} \Omega_{kl}, \quad (51c)$$

$$+ \Omega_{il} \Sigma_{jk} + \Omega_{jk} \Sigma_{il} + \Omega_{jl} \Sigma_{ik} + \Omega_{kl} \Sigma_{ij} + \Omega_{ij} \Omega_{kl}, \quad (51d)$$

for $i, j, k = 1, \dots, d$.

Proof of Proposition 3.4. Introducing the short-hand notation $\rho[h] := \mathbb{E}_{\rho_t}(h) = \int_{\mathbb{R}^d} h(a) \rho_t(da)$, setting $v_t^0 = 0$ and fixing $y \in \mathbb{R}^d$, we first compute the right-hand side $f_{\rho_t, v_t^0}(y)$ of (17b):

$$\begin{aligned} &= \int_{\mathbb{R}^d} (x^\top y + 1)^2 (h(x) - \rho_t[h]) \rho_t(dx) \\ &= \int_{\mathbb{R}^d} (y^\top x x^\top y + 2x^\top y + 1) (h(x) - \rho_t[h]) \rho_t(dx) \\ &= \int_{\mathbb{R}^d} (y^\top x x^\top y + 2x^\top y) (h(x) - \rho_t[h]) \rho_t(dx) \\ &= \int_{\mathbb{R}^d} \left\{ y^\top x x^\top y (h(x) - \rho_t[h]) + 2x^\top y (h(x) - \rho_t[h]) \right\} \rho_t(dx) =: \textcircled{1} + \textcircled{2}, \end{aligned}$$

where we denote

$$\textcircled{1} := \int_{\mathbb{R}^d} y^\top x x^\top y (h(x) - \rho_t[h]) \rho_t(dx) \quad \text{and} \quad \textcircled{2} := \int_{\mathbb{R}^d} 2x^\top y (h(x) - \rho_t[h]) \rho_t(dx).$$

Now we compute

$$\begin{aligned} \textcircled{1} &= \int_{\mathbb{R}^d} y^\top x x^\top y (h(x) - \rho_t[h]) \rho_t(dx) = \int_{\mathbb{R}^d} y^\top x x^\top y (h(x) - \rho_t[h]) \rho_t(dx) \\ &= \int_{\mathbb{R}^d} y^\top x x^\top y \left\{ \frac{1}{2}(Hx - \beta)^\top R^{-1}(Hx - \beta) - \rho_t[h] \right\} \rho_t(dx) \\ &= \frac{1}{2} \int_{\mathbb{R}^d} y^\top x x^\top y x^\top H^\top R^{-1} H x \rho_t(dx) - \frac{1}{2} \int_{\mathbb{R}^d} y^\top x x^\top y x^\top H^\top R^{-1} \beta \rho_t(dx) \\ &\quad - \frac{1}{2} \int_{\mathbb{R}^d} y^\top x x^\top y \beta^\top R^{-1} H x \rho_t(dx) + \frac{1}{2} \int_{\mathbb{R}^d} y^\top x x^\top y \beta^\top R^{-1} \beta \rho_t(dx) \\ &\quad - \int_{\mathbb{R}^d} \frac{1}{2}(Ha - \beta)^\top R^{-1}(Ha - \beta) \rho_t(da) \cdot \int_{\mathbb{R}^d} y^\top x x^\top y \rho_t(dx). \end{aligned}$$

Denote $A := H^\top R^{-1} H$, $B := H^\top R^{-1}$, $M := R^{-1} H$, $D := R^{-1}$ and rewrite $\textcircled{1}$ in indexed form:

$$\begin{aligned} \textcircled{1} &= \frac{1}{2} \mathbb{E}_{X_t} \sum_{i,j,k,l} y_i x_i x_j y_j x_k A_{kl} x_l - \frac{1}{2} \mathbb{E}_{X_t} \sum_{i,j,k,l} y_i x_i x_j y_j x_k B_{kl} \beta_l - \frac{1}{2} \mathbb{E}_{X_t} \sum_{i,j,k,l} y_i x_i x_j y_j \beta_k M_{kl} x_l \\ &\quad + \frac{1}{2} \mathbb{E}_{X_t} \sum_{i,j,k,l} y_i x_i x_j y_j \beta_k D_{kl} \beta_l - \frac{1}{2} \left(\mathbb{E}_{X_t} \sum_{i,j} y_i x_i x_j y_j \right) \left(\mathbb{E}_{X_t} \sum_{k,l} x_k A_{kl} x_l \right) \\ &\quad + \frac{1}{2} \left(\mathbb{E}_{X_t} \sum_{i,j} y_i x_i x_j y_j \right) \left(\mathbb{E}_{X_t} \sum_{k,l} x_k B_{kl} \beta_l \right) + \frac{1}{2} \left(\mathbb{E}_{X_t} \sum_{i,j} y_i x_i x_j y_j \right) \left(\mathbb{E}_{X_t} \sum_{k,l} \beta_k M_{kl} x_l \right) \\ &\quad - \frac{1}{2} \left(\mathbb{E}_{X_t} \sum_{i,j} y_i x_i x_j y_j \right) \left(\mathbb{E}_{X_t} \sum_{k,l} \beta_k D_{kl} \beta_l \right). \end{aligned}$$

Now using Lemma A.1 and the linear properties of expectation and summation, we can compute (1) and simplify:

$$\begin{aligned}
(1) &= \frac{1}{2} \sum_{i,j,k,l} \{ y_i y_j [(A_{kl} C_t^{ik} C_t^{jl} + A_{kl} C_t^{il} C_t^{jk} + A_{kl} \Omega_{ik} C_t^{jl} + A_{kl} \Omega_{il} C_t^{jk} + A_{kl} \Omega_{jk} C_t^{il} + A_{kl} \Omega_{jl} C_t^{ik} \\
&\quad - (B_{kl} \beta_l C_t^{jk} \mu_t^i + B_{kl} \beta_l C_t^{ik} \mu_t^j) - (M_{kl} \beta_k C_t^{jl} \mu_t^i + M_{kl} \beta_k C_t^{il} \mu_t^j)]\} \\
&= \frac{1}{2} y^\top \{ C_t A C_t^\top + C_t A^\top C_t^\top + \Omega A C_t^\top + \Omega A^\top C_t^\top + C_t A \Omega^\top + C_t A^\top \Omega^\top - [\mu_t (C_t B \beta)^\top + (C_t B \beta) \mu_t^\top] \\
&\quad - [\mu_t (C_t M^\top \beta)^\top + (C_t M^\top \beta) \mu_t^\top] \} y = y^\top \{ C_t A C_t + \Omega A C_t + C_t A \Omega - [\mu_t (C_t B \beta)^\top + (C_t B \beta) \mu_t^\top] \} y,
\end{aligned}$$

remind $\Omega_{ij} := \mu_t^i \mu_t^j$. Similarly, we can derive

$$(2) = \sum_{i,j,k} \{ y_i [(A_{jk} \mu_t^j C_t^{ik} + A_{jk} \mu_t^k C_t^{ij}) - B_{jk} \beta_k C_t^{ij} - M_{jk} \beta_j C_t^{ik}] \} = y^\top [2C_t A \mu_t - 2C_t B \beta].$$

We now consider the left-hand side of (17b) with $\varepsilon = 0$:

$$\begin{aligned}
LHS &= \int_{\mathbb{R}^d} \int_{\mathbb{R}^d} (2(x^\top y + 1)y) \cdot C_t (2(x^\top z + 1)z) \alpha_t(z) \rho_t(dx) \rho_t(dz) \\
&= 4 \int_{\mathbb{R}^d} \int_{\mathbb{R}^d} (x^\top y + 1)(x^\top z + 1)y^\top C_t z \alpha_t(z) \rho_t(dx) \rho_t(dz) \\
&= 4 \left(\mathbb{E}_{X_t} \mathbb{E}_{Z_t} \sum_{i,j,k} x_i y_i x_k z_k y_j C_t^{jl} z_l \phi(z) + \mathbb{E}_{X_t} \mathbb{E}_{Z_t} \sum_{i,j} x_i y_i y_j C_t^{jl} z_l \phi(z) \right. \\
&\quad \left. + \mathbb{E}_{X_t} \mathbb{E}_{Z_t} \sum_{i,j} x_i z_i y_j C_t^{jl} z_l \alpha_t(z) + \mathbb{E}_{X_t} \mathbb{E}_{Z_t} \sum_{i,j} y_i C_t^{il} z_l \alpha_t(z) \right),
\end{aligned}$$

where Z is an independent identically distributed copy of X . Defining $(\Psi)_{ij} := \psi_{ij} := -\mathbb{E}_{Z_t}[z_i z_j \alpha_t(z)]$ and $(\eta)_i := \eta_i := -\mathbb{E}_{Z_t}[z_i \alpha_t(z)]$, we can write this as

$$\begin{aligned}
LHS &= -4 \left(\sum_{i,j,k} y_i y_j (C_t^{ik} + \Omega_{ik}) C_t^{jl} \psi_{lk} + \sum_{i,j} y_i y_j \mu_t^i C_t^{jl} \eta_l + \sum_{i,j} y_j \mu_t^i C_t^{jl} \psi_{li} + \sum_i y_i C_t^{il} \eta_l \right) \\
&= -4y^\top ((C_t + \Omega) \Psi C_t + \mu_t \eta^\top C_t) y - 4y^\top (C_t \Psi \mu_t + C_t \eta).
\end{aligned}$$

To solve $LHS = RHS$ for all y , it is equivalent to solve the following system of equations:

$$\begin{cases} C_t (8\Psi + 2A) C_t + \Omega (4\Psi + 2A) C_t + C_t (4\Psi + 2A) \Omega + 8\mu_t \eta^\top C_t + 8C_t \eta \mu_t^\top - 2\mu_t (C_t B \beta)^\top - 2(C_t B \beta) \mu_t^\top = 0, \\ 4(C_t \Psi \mu_t + C_t \eta) + 2C_t A \mu_t - 2C_t B \beta = 0. \end{cases}$$

Subtract the second equation and the transpose of the second equation from the first equation we obtain

$$8C_t \Psi C_t + 2C_t A C_t = 0,$$

which implies

$$\Psi = -\frac{1}{4} A.$$

Substituting this back into the second equation we see that

$$\eta = \frac{1}{2} B \beta - \frac{1}{4} A \mu_t.$$

Finally, we compute the velocity field on the right-hand side of (17a):

$$v(x) = -C_t \int_{\mathbb{R}^d} \nabla_x k(x, z) \alpha_t(z) \rho_t(dz) = -C_t \int_{\mathbb{R}^d} (2(x^\top z + 1)z) \alpha_t(z) \rho_t(dz).$$

In index form this reads

$$v_j(x) = -2 \sum_{i,l} C_t^{jl} x_i \mathbb{E}_{Z_t}[z_i z_l \alpha_t(z)] - 2 \sum_l C_t^{jl} \mathbb{E}_{Z_t}[z_l \alpha_t(z)] = 2 \sum_{i,l} x_i C_t^{jl} \psi_{li} + 2 \sum_l C_t^{jl} \eta_l,$$

write it back to the matrix form:

$$v(x) = -\frac{1}{2}C_t A(x + \mu_t) + C_t B\beta.$$

Recalling that $\mu_t = \mu(\rho_t)$, we substitute the values of A and B back and hence conclude (24). \square

A.3 Proof of Proposition 4.1

Proof. We begin by showing that $J_{\varepsilon,t}$ is well defined on $(L^2(\rho_t))^d$. For that purpose, assume first that v is smooth and compactly supported. In that case, we can write

$$\begin{aligned} \text{MMD}_k^2(\partial_t \rho_t^v, \partial_t \pi_t) &= \left\| \int_{\mathbb{R}^d} k(\cdot, x) \partial_t \rho_t^v(dx) - \int_{\mathbb{R}^d} k(\cdot, x) \partial_t \pi_t(dx) \right\|_{\mathcal{H}_k}^2 \\ &= \int_{\mathbb{R}^d} \int_{\mathbb{R}^d} k(x, y) (\partial_t \rho_t^v(dx) - \partial_t \pi_t(dx)) (\partial_t \rho_t^v(dy) - \partial_t \pi_t(dy)) \\ &= \int_{\mathbb{R}^d} \int_{\mathbb{R}^d} k(x, y) \left(\nabla \cdot (\rho_t v)(x) - \bar{h}(x) \rho_t(x) \right) \left(\nabla \cdot (\rho_t v)(y) - \bar{h}(y) \rho_t(y) \right) dx dy, \end{aligned} \quad (52)$$

where we have introduced the short-hand notation $\bar{h} = h - \int_{\mathbb{R}^d} h d\rho_t$. Using the assumptions on k and h and performing integration by parts, we see that $v \mapsto \text{MMD}_k^2(\partial_t \rho_t^v, \partial_t \pi_t)$ is continuous for the $(L^2(\rho_t))^d$ -topology, and therefore can be extended to $(L^2(\rho_t))^d$. We furthermore see that $J_{\varepsilon,t}$ is quadratic and hence convex in v , and thus there exists a unique minimiser $v^* \in (L^2(\rho_t))^d$.

We now use the regression interpretation suggested by (42) to connect (30) to an appropriate Tikhonov functional [22, Section 2.2]. Following the discussion in Section 4, we consider the operator

$$A = C \nabla : L^2(\rho_t) \rightarrow (L^2(\rho_t))^d$$

and its adjoint $A^* : (L^2(\rho_t))^d \rightarrow L^2(\rho_t)$, given by $A^* v = -\frac{1}{\rho_t} \nabla \cdot (\rho_t v)$. Using the inclusion operator $i : \mathcal{H}_k \hookrightarrow L^2(\rho_t)$ and its adjoint (see Section 4), we consider the operator

$$(Ai)^* : \left((L^2(\rho_t))^d, \langle \cdot, \cdot \rangle_{L^2(\rho_t), C} \right) \rightarrow (\mathcal{H}_k, \langle \cdot, \cdot \rangle_{\mathcal{H}_k}).$$

According to [22, Theorem 2.11], and using the Woodbury (or ‘push-through’) identity, it follows that v^* as in (42) minimises the Tikhonov functional

$$\|i^*(A^* v - \bar{h})\|_{\mathcal{H}_k}^2 + \|v\|_{L^2(\rho_t), C}^2. \quad (53)$$

To finish the proof, it is thus sufficient to show that $\|i^*(A^* v - \bar{h})\|_{\mathcal{H}_k}^2 = \text{MMD}_k^2(\partial_t \rho_t^v, \partial_t \pi_t)$. For this, notice that

$$\|i^* f\|_{\mathcal{H}_k}^2 = \int_{\mathbb{R}^d} \int_{\mathbb{R}^d} f(x) k(x, y) f(y) \rho_t(dx) \rho_t(dy), \quad (54)$$

by [49, Theorem 4.26]. The claim follows by comparing (54) with (52), and using the expression for A^* . \square

B Bibliography

- [1] A. Bain and D. Crisan. *Fundamentals of stochastic filtering*, volume 3. Springer, 2009.
- [2] K. Bergemann and S. Reich. A localization technique for ensemble Kalman filters. *Quarterly Journal of the Royal Meteorological Society: A journal of the atmospheric sciences, applied meteorology and physical oceanography*, 136(648):701–707, 2010.
- [3] K. Bergemann and S. Reich. A mollified ensemble Kalman filter. *Quarterly Journal of the Royal Meteorological Society*, 136(651):1636–1643, 2010.

- [4] B. Boots, G. Gordon, and A. Gretton. Hilbert space embeddings of predictive state representations. In *Proceedings of the Twenty-Ninth Conference on Uncertainty in Artificial Intelligence, UAI 2013, Bellevue, WA, USA, August 11-15, 2013*. AUAI Press, 2013.
- [5] E. Calvello, S. Reich, and A. M. Stuart. Ensemble Kalman methods: A mean field perspective. *arXiv preprint arXiv:2209.11371*, 2022.
- [6] Y. Chen, D. Z. Huang, J. Huang, S. Reich, and A. M. Stuart. Gradient flows for sampling: Mean-field models, gaussian approximations and affine invariance. *arXiv preprint arXiv:2302.11024*, 2023.
- [7] M. Coghi, T. Nilssen, N. Nüsken, and S. Reich. Rough McKean–Vlasov dynamics for robust ensemble Kalman filtering. *The Annals of Applied Probability*, 33(6B):5693–5752, 2023.
- [8] R. R. Coifman and S. Lafon. Diffusion maps. *Applied and computational harmonic analysis*, 21(1):5–30, 2006.
- [9] A. Duncan, N. Nüsken, and L. Szpruch. On the geometry of Stein variational gradient descent. *Journal of Machine Learning Research*, 24:1–39, 2023.
- [10] G. Evensen, F. C. Vossepoel, and P. J. van Leeuwen. *Data assimilation fundamentals: A unified formulation of the state and parameter estimation problem*. Springer Nature, 2022.
- [11] A. Figalli and F. Glaudo. *An invitation to optimal transport, Wasserstein distances, and gradient flows*. EMS press, 2021.
- [12] K. Fukumizu, F. R. Bach, and M. I. Jordan. Dimensionality reduction for supervised learning with reproducing kernel Hilbert spaces. *Journal of Machine Learning Research*, 5(Jan):73–99, 2004.
- [13] K. Fukumizu, A. Gretton, X. Sun, and B. Schölkopf. Kernel measures of conditional dependence. *Advances in neural information processing systems*, 20, 2007.
- [14] K. Fukumizu, L. Song, and A. Gretton. Kernel Bayes’ rule: Bayesian inference with positive definite kernels. *The Journal of Machine Learning Research*, 14(1):3753–3783, 2013.
- [15] A. Garbuno-Ingó, N. Nüsken, and S. Reich. Affine invariant interacting langevin dynamics for bayesian inference. *SIAM Journal on Applied Dynamical Systems*, 19(3):1633–1658, 2020.
- [16] G. Gebhardt, A. Kupcsik, and G. Neumann. The kernel Kalman rule—efficient nonparametric inference with recursive least squares. In *Proceedings of the AAAI Conference on Artificial Intelligence*, volume 31, 2017.
- [17] G. H. Gebhardt, A. Kupcsik, and G. Neumann. The kernel Kalman rule: Efficient nonparametric inference by recursive least-squares and subspace projections. *Machine Learning*, 108(12):2113–2157, 2019.
- [18] J. Goodman and J. Weare. Ensemble samplers with affine invariance. *Communications in applied mathematics and computational science*, 5(1):65–80, 2010.
- [19] S. Grünewälder, G. Lever, A. Gretton, L. Baldassarre, S. Patterson, and M. Pontil. Conditional mean embeddings as regressors. In *Proceedings of the 29th International Conference on Machine Learning, ICML 2012, Edinburgh, Scotland, UK, June 26 - July 1, 2012*, 2012.
- [20] J. Heng, A. Doucet, and Y. Pokern. Gibbs flow for approximate transport with applications to Bayesian computation. *Journal of the Royal Statistical Society Series B: Statistical Methodology*, 83(1):156–187, 2021.
- [21] M. Kanagawa, P. Hennig, D. Sejdinovic, and B. K. Sriperumbudur. Gaussian processes and kernel methods: A review on connections and equivalences. *arXiv preprint arXiv:1807.02582*, 2018.
- [22] A. Kirsch et al. *An introduction to the mathematical theory of inverse problems*, volume 120. Springer, 2011.

[23] I. Klebanov, I. Schuster, and T. J. Sullivan. A rigorous theory of conditional mean embeddings. *SIAM Journal on Mathematics of Data Science*, 2(3):583–606, 2020.

[24] M. Kuang and E. G. Tabak. Sample-based optimal transport and barycenter problems. *Communications on Pure and Applied Mathematics*, 72(8):1581–1630, 2019.

[25] K. Law, A. Stuart, and K. Zygalakis. *Data assimilation: A mathematical introduction*. Springer, 2015.

[26] Q. Liu and D. Wang. Stein variational gradient descent: A general purpose Bayesian inference algorithm. *Advances in neural information processing systems*, 29, 2016.

[27] S. Livingstone and M. Girolami. Information-geometric markov chain monte carlo methods using diffusions. *Entropy*, 16(6):3074–3102, 2014.

[28] A. Maurais and Y. Marzouk. Adaptive algorithms for continuous-time transport: Homotopy-driven sampling and a new interacting particle system. In *NeurIPS 2023 Workshop Optimal Transport and Machine Learning*, 2023.

[29] A. Maurais and Y. Marzouk. Sampling in unit time with kernel Fisher-Rao flow. *arXiv preprint arXiv:2401.03892*, 2024.

[30] J. Michalowicz, J. Nichols, F. Bucholtz, and C. Olson. An isserlis’ theorem for mixed gaussian variables: Application to the auto-bispectral density. *Journal of Statistical Physics*, 136:89–102, 2009.

[31] K. Muandet, K. Fukumizu, B. Sriperumbudur, B. Schölkopf, et al. Kernel mean embedding of distributions: A review and beyond. *Foundations and Trends® in Machine Learning*, 10(1-2):1–141, 2017.

[32] Y. Nishiyama, A. Boulieras, A. Gretton, and K. Fukumizu. Hilbert space embeddings of POMDPs. In N. de Freitas and K. P. Murphy, editors, *Proceedings of the Twenty-Eighth Conference on Uncertainty in Artificial Intelligence, Catalina Island, CA, USA, August 14-18, 2012*, pages 644–653. AUAI Press, 2012.

[33] N. Nüsken and D. M. Renger. Stein variational gradient descent: Many-particle and long-time asymptotics. *Foundations of Data Science*, 5(3):286–320, 2023.

[34] S. Pathiraja, S. Reich, and W. Stannat. McKean–Vlasov SDEs in nonlinear filtering. *SIAM Journal on Control and Optimization*, 59(6):4188–4215, 2021.

[35] S. Pathiraja and W. Stannat. Analysis of the feedback particle filter with diffusion map based approximation of the gain. *arXiv preprint arXiv:2109.02761*, 2021.

[36] G. A. Pavliotis. *Stochastic processes and applications*. Springer, 2016.

[37] L. Pillaud-Vivien and F. Bach. Kernelized diffusion maps. *arXiv preprint arXiv:2302.06757*, 2023.

[38] M. Pulido and P. J. van Leeuwen. Sequential Monte Carlo with kernel embedded mappings: The mapping particle filter. *Journal of Computational Physics*, 396:400–415, 2019.

[39] S. Reich. A dynamical systems framework for intermittent data assimilation. *BIT Numerical Mathematics*, 51:235–249, 2011.

[40] S. Reich and C. Cotter. *Probabilistic forecasting and Bayesian data assimilation*. Cambridge University Press, 2015.

[41] S. Reich and C. J. Cotter. Ensemble filter techniques for intermittent data assimilation. *Large Scale Inverse Problems: Computational Methods and Applications in the Earth Sciences*, 13:91–134, 2013.

[42] A. Smola, A. Gretton, L. Song, and B. Schölkopf. A Hilbert space embedding for distributions. In *International conference on algorithmic learning theory*, pages 13–31. Springer, 2007.

- [43] A. J. Smola and B. Schölkopf. *Learning with kernels*, volume 4. Citeseer, 1998.
- [44] L. Song, B. Boots, S. M. Siddiqi, G. J. Gordon, and A. J. Smola. Hilbert space embeddings of hidden Markov models. In J. Fürnkranz and T. Joachims, editors, *Proceedings of the 27th International Conference on Machine Learning (ICML-10), June 21-24, 2010, Haifa, Israel*, pages 991–998. Omnipress, 2010.
- [45] L. Song, K. Fukumizu, and A. Gretton. Kernel embeddings of conditional distributions: A unified kernel framework for nonparametric inference in graphical models. *IEEE Signal Processing Magazine*, 30(4):98–111, 2013.
- [46] L. Song, J. Huang, A. Smola, and K. Fukumizu. Hilbert space embeddings of conditional distributions with applications to dynamical systems. In *Proceedings of the 26th Annual International Conference on Machine Learning*, pages 961–968, 2009.
- [47] B. K. Sriperumbudur, K. Fukumizu, and G. R. Lanckriet. Universality, characteristic kernels and RKHS embedding of measures. *Journal of Machine Learning Research*, 12(7), 2011.
- [48] B. K. Sriperumbudur, A. Gretton, K. Fukumizu, B. Schölkopf, and G. R. Lanckriet. Hilbert space embeddings and metrics on probability measures. *The Journal of Machine Learning Research*, 11:1517–1561, 2010.
- [49] I. Steinwart and A. Christmann. *Support vector machines*. Springer Science & Business Media, 2008.
- [50] A. S. Stordal, R. J. Moraes, P. N. Raanes, and G. Evensen. p-kernel Stein variational gradient descent for data assimilation and history matching. *Mathematical Geosciences*, 53(3):375–393, 2021.
- [51] M. Sun, M. E. Davies, I. K. Poudler, and J. R. Hopgood. Adaptive kernel Kalman filter. *IEEE Transactions on Signal Processing*, 71:713–726, 2023.
- [52] S. Syed. *Non-reversible parallel tempering on optimized paths*. PhD thesis, University of British Columbia, 2022.
- [53] S. Syed, V. Romaniello, T. Campbell, and A. Bouchard-Côté. Parallel tempering on optimized paths. In *International Conference on Machine Learning*, pages 10033–10042. PMLR, 2021.
- [54] A. Taghvaei, J. De Wiljes, P. G. Mehta, and S. Reich. The Kalman filter and its modern extensions for the continuous-time nonlinear filtering problem. *Journal of Dynamic Systems, Measurement, and Control*, 140(3):030904, 2018.
- [55] A. Taghvaei, P. G. Mehta, and S. P. Meyn. Diffusion map-based algorithm for gain function approximation in the feedback particle filter. *SIAM/ASA Journal on Uncertainty Quantification*, 8(3):1090–1117, 2020.
- [56] M. J. Wainwright. *High-dimensional statistics: A non-asymptotic viewpoint*, volume 48. Cambridge university press, 2019.
- [57] L. Xu, Y. Chen, A. Doucet, and A. Gretton. Importance weighting approach in kernel Bayes’ rule. *arXiv preprint arXiv:2202.02474*, 2022.
- [58] T. Yang, P. G. Mehta, and S. P. Meyn. Feedback particle filter. *IEEE transactions on Automatic control*, 58(10):2465–2480, 2013.